MAGNETIC NOISE, BARKHAUSEN EFFECT

The change of the magnetic state of a ferro- or ferrimagnetic body under the effect of a slowly changing externally applied magnetic field is a complex process, involving reversible and irreversible changes of the magnetization. Due to irreversible magnetization processes, any change of the magnetic state is accompanied by losses, manifested in the presence of the magnetic hysteresis. The reason for the losses is that any real material has a defect structure, responsible for the details of the hysteresis loop. The magnetization changes discontinuously, by jumps from defect to defect, giving rise to magnetic noise, which can be made audible through a headphone. This process and the corresponding noise is named after its discoverer, H. Barkhausen (1919) as *Barkhausen jumps* and *Barkhausen noise.*

The magnetization process (M) of a ferromagnetic (or ferrimagnetic) body is represented by a nonlinear and multivalued function of the applied magnetic field (H), the magnetic hysteresis loop. Figure 1 shows the magnetic hysteresis loop of a magnetic composite of nanometer size iron particles embedded in a nonmagnetic ZnO matrix. At any given temperature the maximum attainable magnetization is called the saturation, or spontaneous magnetization, M_s. Reducing the magnetic field from saturation to $H = 0$ brings the magnetic body to the remanent state with the remanent magnetization (or remanence) of M_r. Further reducing the field in the negative direction down to the coercive field (coercivity), at $-H = -H_c$, the magnetization will be reduced to $M = 0$.

The equilibrium state of the magnetization corresponds to the minimum of the free energy of the magnetic material. The most important contributions to the free energy are due to (1) the quantum mechanical exchange energy, responsible for the collective ordering of the individual spin magnetic moments of the electrons; (2) the magnetocrystalline anisotropy energy, favoring some crystalline directions for the magnetization direction with respect to others, giving rise to the easy and hard directions of magnetization; (3) magnetostrictive stresses, that is, the length change of a magnetic material in the presence of mechanical stress; (4) the Zeeman energy of the interaction with the externally applied magnetic field(s); (5) the magnetostatic energy due to the creation of internal and external demagnetizing fields, depending on the shape and size of the magnetic body; and (6) the energy of interaction of the magnetization with defects in the magnetic body. Due to (6)

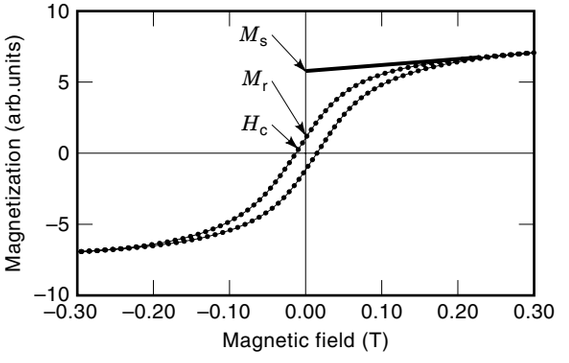

Figure 1. Magnetic hysteresis loop of a nanocomposite of iron in ZnO. M_s saturation magnetization, M_r remanent magnetization, H_c coercivity (M. Pardavi-Horvath, unpublished data).

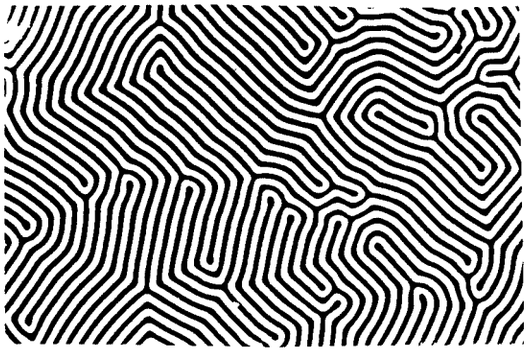

Figure 2. Magnetic domain structure in $H = 0$ applied magnetic field of a defect-free 5 μm thin single crystalline yttrium iron garnet film. The magneto-optic contrast is due to the opposite direction of the magnetization in black-and-white domains with respect to the surface normal. The periodicity of the domain structure in 10 μm (Microphotograph in polarized light).

the details of the magnetization curve of two apparently similar pieces of the same magnetic material might differ substantially. In the absence of any applied magnetic field, the equilibrium state of a magnetic body would be that of zero magnetization. The existence of the remanent magnetization, the basis of the operation of any permanent magnet or magnetic recording device, is the result of the defect structure in the material, and/or shape and size distribution of the particles or grains. These features are controlled by the technology of manufacturing the material. However, any magnetic material can be brought to the $M = 0$ state in $H = 0$, by demagnetizing it. The most frequent process of demagnetization is to apply an ac magnetic field of an amplitude large enough to saturate the material, and slowly and gradually reduce the amplitude to zero.

In the demagnetized state the distribution of the magnetization inside of the magnetic body is nonuniform. The magnetic structure consists of domains, small regions of different magnetization direction (1). The vectorial sum of all of the domain magnetizations is zero in the absence of any applied magnetic field. The geometry and the size of the domain structure is governed by the interactions, delineated previously. The domain structure can be observed by a number of techniques, including magnetic force microscopy, Lorentz electron microscopy, or in polarized light, utilizing the magneto-optic Faraday or Kerr effects. In some cases the domain structure can be very simple, consisting of only two sets of domains, magnetized "up" and "down," as in the case of a 5 μm thin, single crystalline ferrimagnetic garnet sample, a microphotograph of which, taken in polarized light via the magneto-optic Faraday effect, is shown in Fig. 2. The areas of dark and light contrast correspond to the directions of the magnetization perpendicular to the sample surface, directed "downward" and "upward," respectively. In $H = 0$ the two regions have equal volumes, such that the total magnetization $M = 0$. The boundary line between the domains is the domain wall (DW), where the direction of the magnetization is changing gradually between the two domains whose magnetization directions differ by 180°. The size and shape of the domains and the position of the DWs correspond to the minimum free energy configuration. In a flawless material the domain structure is very regular by crystal symmetry, as seen in Fig. 2 for a single crystal grown along the [111] crystalline direction. The threefold symmetry of that axis is evident.

Upon applying an external magnetic field to a previously demagnetized magnetic body, its magnetization follows the initial (virgin) magnetization curve. Assuming a perfectly homogeneous, flawless material without any preferred axis, the process of magnetization change might proceed reversibly, with no losses involved (1,2). In such a case, the field will exert a force on the domain magnetizations and increase the magnetizations of the domains lying near to the field direction by increasing their volume. This magnetization change happens via the motion of the DWs to new positions. This wall motion is reversible up to a certain magnetic field value and if the field is reduced to zero, the walls move back to their original position and M returns to zero ($M_r = 0$) in $H = 0$. In an ideally perfect material this reversible wall motion would dominate the magnetization process up to magnetic field values near to saturation. Then the magnetization vectors of the remaining domains would start turning into the direction of the field, completing the magnetization process by rotation. This magnetization process is illustrated in Fig. 3. For a thin slab of a magnetic material, having an easy axis of the magnetization along the side of slab, the magnetic field is applied along this easy axis.

In any real material there are always microstructural defects: inclusions of foreign phases, voids, dislocations, inhomogeneous stresses, irregular surfaces and interfaces, grain boundaries, cracks, and so on, such that the free energy of the material is not uniform over the body, and the conditions for magnetization change will vary locally. The free energy might have local minima (or maxima) at some defects, where the DWs will be pinned. They can only move and increase (decrease) the magnetization when the magnetic field changes enough to provide a force sufficient to overcome the energy barriers between the defects. The domain wall will then discontinuously jump from one pinned position to another. The irreversible processes of discontinuous DW displacement are

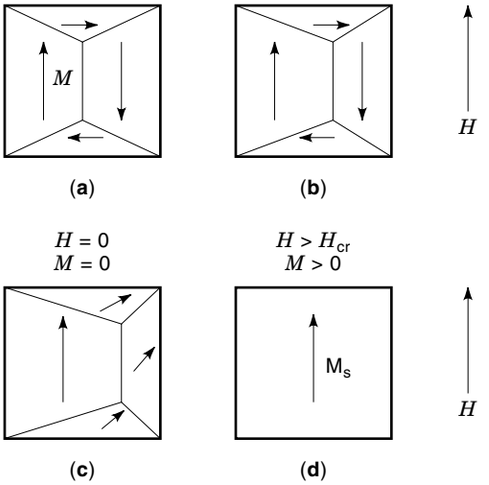

Figure 3. Magnetization processes by wall motion and rotation. (a) Demagnetized state: $\boldsymbol{H} = \boldsymbol{0}$, $\boldsymbol{M} = \boldsymbol{0}$; (b) Irreversible wall motion: $\boldsymbol{H} > \boldsymbol{0}$, domains having favorable magnetization direction with respect to the applied magnetic field are growing; (c) The magnetization in domains with unfavorable direction is rotating toward the magnetic field direction; (d) Saturation: domains disappeared, magnetization aligned with the applied field.

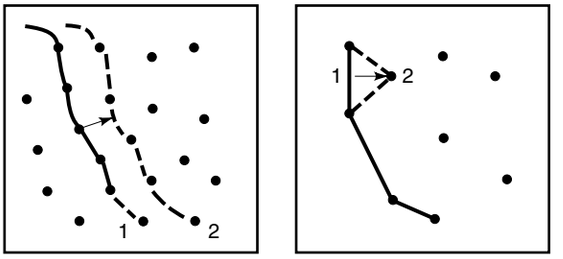

Figure 4. Magnetization change by irreversible wall motion: Barkhausen jumps of domain walls (lines) pinned at defects (dots). (a) Wall pinned at many defects, simultaneous breakaway with a large magnetization jump. (b) Domain wall motion by individual jumps from defect to defect. 1 is the original DW position in $H = 0$; 2 is the DW position in $H > H_{cr}$.

called Barkhausen jumps. In a macroscopic body, the defects are distributed more or less randomly in space and energy. When the magnetic field reaches the critical value for the irreversible DW motion of the weakest defect, $H = H_{cr}$, the wall will move until it reaches the next defect, where it will be pinned again. Upon increasing the field there might be another DW pinned at another defect, having a critical field equal to the applied field, and now that wall will jump to the next available energy minimum, and it will be pinned at the next defect. Depending on the density of the defects and the strength of the interaction between defects and DWs, it might happen that a wall will be pinned by many similar defects and it will move, breaking away from many defects simultaneously, giving rise to a large magnetization jump. Figure 4 shows these two different scenarios for Barkhausen jumps. Figure 5 shows strong DW pinning at inclusions in a garnet crystal, near magnetic saturation. The applied field is high enough to reduce the black domains to a very small area, but it is not enough to overcome H_{cr} of the inclusions.

A finite size ferromagnetic material is usually broken into many magnetic domains. Any material, including the demagnetized state, is not, in general, a unique state, as there is a very large number of possible domain arrangements summing to a particular $\boldsymbol{M}$ value. Consequently, the sequence of the Barkhausen jumps is probabilistic. Moreover, the critical field for a jump depends not only on the strength of the actual defect-DW interaction, but on the magnetic state of the neighboring domains too. These domains, like small magnets, create their own magnetic fields at the site of their neighbors (magnetostatic, dipole fields). Depending on the direction of the magnetization of a given domain, it can help or prevent the externally applied magnetic field in supplying the energy for the jump. This energy, needed to overcome the barriers caused by the defects, results in hysteresis losses.

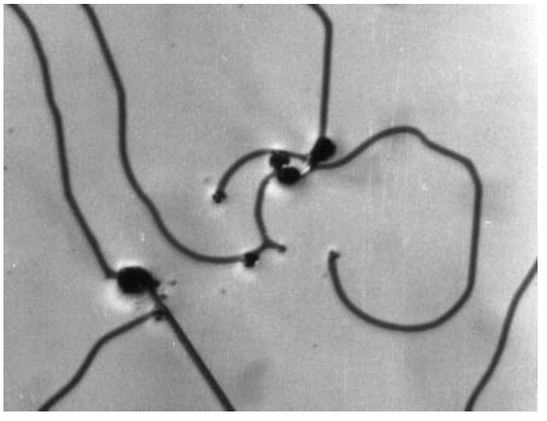

Figure 5. Strong domain wall pinning at inclusions in an epitaxial garnet crystal in applied magnetic field near to saturation, where the magnetization $M = M_{up} - M_{down} \leq M_s$. The black stripe domains correspond to M_{down}. Upon applying a magnetic field $H \gg H_c$, most of the walls disappear, only those pinned by the strongest defects (black dots) are left.

The discrete and irregular nature of the magnetization process causes hysteresis loss and noise in magnetic devices. To reduce these losses, the material should be uniform. The losses can be reduced, even in the presence of a large defect density, if the defects are uniformly distributed and/or they interact very weakly with the moving DWs. In this case the DWs are moving smoothly across the material, with no sudden jumps in the magnetization. The other limiting case is when the material has a very narrow distribution of defects yielding a rectangular hysteresis loop. In contrast, for a good permanent magnet very active and strong pinning centers have to be created to keep the magnetization from changing, that is, avoid spontaneous demagnetization.

EQUILIBRIUM MAGNETIZATION DISTRIBUTION

Domains and Domain Walls

The equilibrium state of the macroscopic magnetization of any magnetic body is the state with minimum total free energy (1–5). The term in the free energy responsible for the existence of ordered magnetic states is the exchange interaction between the electrons' magnetic moments. The magnitude of the atomic magnetic moments is constant at a given temperature. The atomic magnetic moments are rendered parallel (antiparallel) to each other due to the exchange interaction, giving rise to ferromagnetic (antiferromagnetic, ferrimagnetic) order. The thermal energy tends to randomize the direction of the atomic magnetic moments, and at the Curie temperature, T_c, it overcomes the exchange energy, and there is no magnetic order above T_c. The magnitude of T_c is proportional to A, the exchange constant, characterizing the strength of the exchange interaction. For iron, $A = 1.49 \times 10^{-11}$ J/m.

The origin of magnetocrystalline anisotropy energy is the interaction between crystalline electric fields and atomic magnetic moments (spin-orbit coupling), rendering these moments parallel to certain, easy crystallographic directions. The simplest form of the magnetocrystalline anisotropy is the uniaxial anisotropy, with one easy axis. The anisotropy energy density can be characterized by a single anisotropy constant K_u. For the hexagonal, uniaxial cobalt at room temperature $K_u = 4.1 \times 10^5$ J/m^3. For cubic crystals the anisotropy is weaker and characterized by two constants, K_1 and K_2, where usually $K_2 \ll K_1$. For iron $K_1 = 4.8 \times 10^4$ J/m^3.

In the absence of an applied magnetic field, the equilibrium state of the distribution of the atomic moments can be found from the minimalization of the total energy, that is, it is determined by the competition of the anisotropy and ex-

change energies, giving rise to the magnetic domain structure. The change of the magnetization direction between adjacent domains is not abrupt, because it would require a large investment of energy against the exchange energy. However, if the transition is very broad then many magnetic moments would be along unfavorable directions from the point of view of anisotropy energy. The result is the minimum energy situation with a formation of a DW of width:

$$\delta_w = \pi\sqrt{A/K}$$

To create a DW, a new, magnetic surface has to be formed. This surface energy of the DW energy is given by:

$$\gamma_w = 4\sqrt{AK}$$

There are other contributions to the free energy of a magnetized body, which have to be taken into account when calculating the distribution of the magnetization. These are the magnetostrictive stresses, the Zeeman energy of the interaction with applied magnetic field, and the magnetostatic energy due to production of demagnetizing fields, depending on the shape and size of the magnetic body.

The total magnetization of the body is the vector sum of the domain magnetizations, $\boldsymbol{M} = \Sigma \boldsymbol{m}_i v_i$, where $\boldsymbol{m}_i$ is the magnetization vector in each domain directed along ϕ_i with respect to field direction, and v_i is the volume of the ith domain. A magnetic material is saturated when all the atomic magnetization vectors are parallel to the applied magnetic field ($e_i = \cos\phi_i = 0$), that is, all the domain magnetizations are turned into the field direction $\boldsymbol{M} = \boldsymbol{M}_s$. (See Fig. 3.) Before saturation any change of the total magnetization can be described by:

$$\delta\boldsymbol{M} = \delta\sum \boldsymbol{m}_i v_i = \sum \boldsymbol{e}_i \delta|m_i| + \sum \boldsymbol{e}_i \delta v_i + \sum v_i |m_i| \delta\boldsymbol{e}$$

The first term is zero because the magnitude of the magnetic moments is constant; the second term describes the change of the volume of the domains via DW motion, and the third term is the contribution of the rotation of the magnetization angle ϕ_i, inside the domains to the change the magnetization.

DOMAIN WALL—DEFECT INTERACTION

Domain Wall Pinning Coercivity

The equilibrium magnetization distribution in any $\boldsymbol{H}$ field is expected to be determined by the minimum energy configuration, when all the contributing energies are taken into account. In a perfectly uniform material the DW energy is the same everywhere and the position and the distance between the DWs is uniform. However, real materials are not uniform. Material properties differ from point to point, and as a consequence, the material constants A and K are not constants, but they are functions of the position $\boldsymbol{r}$: $A(\boldsymbol{r})$ and $K(\boldsymbol{r})$. The result is that at some sites the DW energy is locally lowered (or increased) and extra energy is needed to move the wall from that position, that is, to change the magnetization. In a one-dimensional case, the energy needed to move a DW of volume v ($v = hL\delta_w$, height h, length L, width δ_w, specific DW energy γ_w) by dx has to be compensated by the change of the total DW energy (5,6):

$$\begin{aligned} 2HMdx &= d(v\gamma_w) \\ &= \gamma_w\, dv + v d(\gamma_w) \simeq \gamma_w d(hL\delta_w) + v d\sqrt{A(x)K(x)} \end{aligned}$$

The critical field for the start of the motion of a given DW, that is, the first Barkhausen jump, is:

$$H_{cr} = \frac{1}{2M_s}\frac{d(v\gamma_w)}{dx}$$

For the whole material, the average critical field, that is, the coercive force of the start of the DW motion, for the case when the DW volume remains constant, is given by the rms value of the critical fields of all defects:

$$H_c = \overline{H_{cr}^2}^{1/2} = \frac{1}{2hLM_s}\overline{(d\gamma_w/dx)^2}^{1/2}$$

Thus the necessary condition for the occurrence of Barkhausen jumps is the presence of a gradient of the DW energy. Figure 6 shows a one-dimensional sketch of the energy landscape of a magnetic body, due to the gradient of the DW energy. The DW is located in an energy minimum, pinned by the defect. Upon reaching the critical field of interaction with a defect, the DW breaks away, jumping to a new metastable equilibrium position. The DW can freely move and the magnetization changes continuously if the defects along its path are weaker than the previous maximum in the gradient. The variation of the DW volume across the surface might have a significant contribution to hysteresis losses due to surface roughness effects, as in the case of soft magnetic thin films in recording heads (6).

The change of the DW energy due to local variations of anisotrophy and exchange energy causes DW pinning at localized defects. These defects are responsible for Barkhausen jumps and hysteresis losses. During the magnetization process the energy from the applied magnetic field has to over-

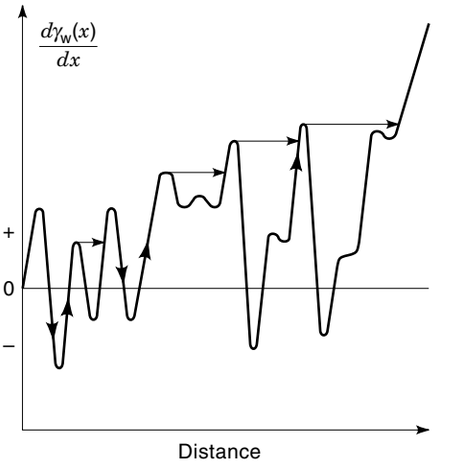

Figure 6. One-dimensional variations of the DW energy landscape of a magnetic body due to the position dependence of anisotropy and exchange energies, caused by localized crystalline defects. Arrows denote the jump of the domain walls to the next position of equal energy.

come the energy of interaction of the moving domain wall with defects in the magnetic body. Due to the statistical nature of the defect distribution, the magnetization curve of two apparently similar pieces of the same magnetic material might differ substantially, depending on the technology of production. Figure 7 is a measured hysteresis loop of 25 quasi-identical magnetic garnet particles. Each particle is seen to be magnetized at different fields, illustrating the distribution of critical fields (7). The mean value of the critical fields for DW motion is scaled with the coercivity of the material. However, for the macroscopic critical field, the coercivity is a statistical parameter, and it has a certain distribution and standard deviation. The standard deviation of the critical field distribution characterizes the spectrum of the defects based on the strength of DW-defect interaction. More accurate, statistical models, given in Ref. 5, take into account that the process of pinning/depinning takes place only over a distance of one domain width w_d, so there will be a $\ln(w_d/\delta_w)$ factor in all formulas for DW pinning. If the defect size is very small (10^{-7} m) compared to the DW width, then the moving DW averages out the defect potential, and there is no irreversible magnetization and hysteresis loss associated with a very fine microstructure. On the other hand, when the defects are very large compared to δ_w, then the energy associated with the inclusions will be reduced due to the presence of secondary domain structure and the associated discontinuous DW motion will be negligibly small and the irreversible magnetization losses will be reduced.

Inhomogeneous Stress Fields

One of the main contributors to Barkhausen noise is related to the stress sensitivity of magnetic materials. The magnetoelastic behavior is characterized by the magnetostrictive strain $\lambda = dl/l$, the relative shape and size change of a magnetized body upon change of the magnetization, or vice versa the change of magnetization upon deformation (1, 5). For single crystals the strain might be different in different crystallographic $\{hkl\}$ directions, with different λ_{hkl}. For polycrystalline materials the average value of λ is used. For most of the magnetic materials $\lambda \cong 10^{-5}$ to 10^{-6}. Elastic stresses σ couple to magnetostriction causing an effective stress-induced anisotropy of the material:

$$K_\sigma = -\frac{3}{2}\lambda\sigma\cos^2\phi$$

where ϕ is the direction of the stress relative to the magnetization. The total anisotropy of the magnetic body is the sum of the magneto-crystalline and stress-induced parts: $K = K_u + K_\sigma$. Localized fluctuations of the internal stresses $\sigma(\boldsymbol{r})$ cause fluctuations in the DW energy through $K(\boldsymbol{r})$ and contribute to the coercivity, that is, to the critical fields for Barkhausen jumps.

If there are long range one-dimensional stress fluctuations $\sigma(x)$ in the material, with an average spatial periodicity (wavelength) Λ, large compared to the DW width, then the DW energy will fluctuate as

$$\gamma_w = 4\sqrt{A[K_u + (3/2)\lambda\sigma(x)]}$$

causing a critical field for the DW motion of:

$$H_{cr}^{\sigma} = \frac{3\lambda\sigma_w(x)}{4M_s}\frac{d\sigma(x)}{dx}$$

This is the basic equation of the stress theory of Barkhausen jumps and coercivity. If $\sigma(x)$ is known then H_{cr} can be calculated.

Assuming a quasi-sinusoidal stress field with an amplitude of $(\sigma_0 \pm \Delta\sigma/2)$ in the form of

$$\sigma(x) = \sigma_0 + \frac{\Delta\sigma}{2}\sin(2\pi x/\Lambda)$$

the critical field for the start of the DW motion is given by

$$H_{cr}^{\sigma} = p\frac{\lambda\overline{|\sigma_i|}}{2M_s}$$

where p depends on the ratio of σ_w/Λ. Although the usual effect of the stress fields of the defects is that the anisotropy of the material is locally reduced, thus creating an effective energy well for the DW, it was demonstrated that it is possible to have anisotropy barriers with locally higher DW energy, preventing the change of the magnetization very efficiently (8). Figure 8 shows such a case, where the stress field from an inclusion in the nonmagnetic substrate penetrates a magnetic crystal and the DWs are repulsed by both stress fields, preventing saturation of the magnetization at fields much higher than the theoretical saturation field.

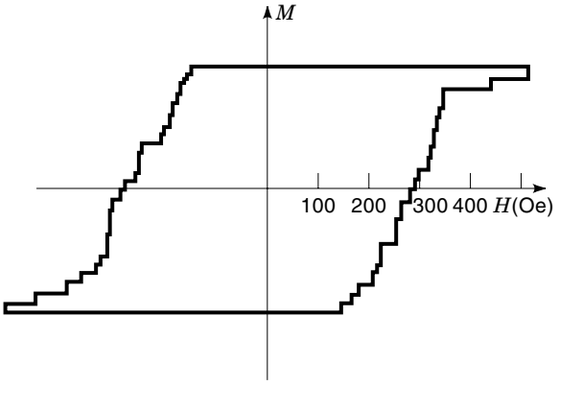

Figure 7. Measured hysteresis loop of 25 quasi-identical magnetic garnet particles, illustrating the sequence of Barkhausen jumps corresponding to the distribution of critical fields of individual particles. (From Ref. 8.)

Domain Wall Interaction with Dislocations

A special case of the stress effects on magnetization processes is due to the presence of dislocations (9,10,11,12,13,14). Plastic deformation produces defects, such as dislocations, stacking faults, and point defects, each associated with an internal stress field, which will affect the Barkhausen noise. For low deformation the number of dislocations increases linearly with shear stress τ, and depends on the material's shear modulus G and the magnitude of the Burgers vector $\mathbf{b}$ characterizing the dislocation. The moving DW interacts with the stress field of the dislocation, depending on the direction and the distance between them. The dislocation exerts a force $\boldsymbol{f}$

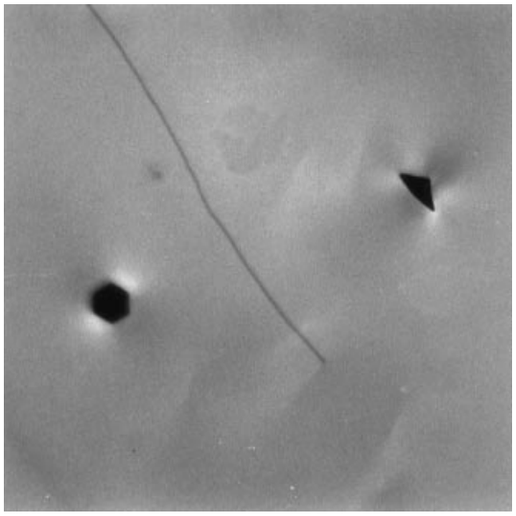

Figure 8. Repulsion of domain walls in a magnetic garnet material by the stress fields of triangular and hexagonal Ir inclusions, originating in the nonmagnetic substrate. The inclusion's stress field penetrates the magnetic layer and interacts with the domain walls. The sample is near saturation, only the thin black domain remains due to the very strong interaction with the stress field.

upon the DW according to its line element $\boldsymbol{dl}$ and the magnetostrictive stress tensor σ of the DW: $\boldsymbol{f} = -\boldsymbol{dl} \times \sigma\mathbf{b}$. The calculation of this interaction for a general case is not trivial.

For a simple case of a 180° DW, lying in the $x-y$ plane and a dislocation running parallel to the plane of the DW, the geometry shown in Fig. 9, the critical field is calculated in Ref. 10. For the simple case of the change of the magnetization across the DW $\phi = \pi/\delta_w$, $\theta = 0$. The edge and screw components of the dislocations are $b\sin\alpha$ and $b\cos\alpha$. For an edge dislocation $\alpha = \omega = 90°$, for a screw dislocation $\alpha = 0$. For a dislocation running parallel to the x axis $\epsilon = 0$. The angle between **b** and the z axis is ω. The component of the force f_z is given as

$$f_z = (3/2)Gb\lambda(\sin 2\phi\cos\alpha + 2\sin^2\phi\sin\omega\sin\alpha)$$

The DW interacts with the dislocation only as long as the dislocation is inside of the wall, because $f_z = 0$ for $\phi = 0$, consequently, $f_{max} = (3/2)\ Gb\lambda$. To move the DW by dz, $dW = f\ dz$ work should be performed. The energy necessary

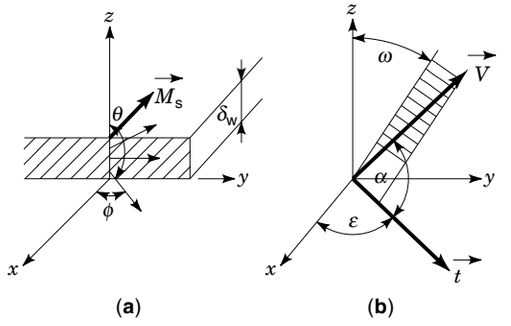

Figure 9. Geometry of the DW dislocation interaction. M_s saturation magnetization, δ_w DW width, V Burger's vector of the dislocation.

to get the whole DW over the single dislocation barrier is $W = (3/2)\ Gb\sigma_w\lambda$. The critical field for the DW motion from a single straight edge dislocation is:

$$H_{cr}^{d} = (3/2M_s)Gb\lambda$$

For a dislocation density of N m^{-2} H_{cr} will be proportional to $N^{1/2}$, that is, the linear defect density.

In some cases the measured H_{cr} is much higher than the expected from the above equation. This is due to the fact that, depending on material parameters, the DW might be elastically deformed, that is, stretched between two dislocations before breaking free (1,5,15). Assuming that the amplitude of DW bulging is one-quarter of the distance between dislocations, the critical field for the DW jump is:

$$H_{cr}^{d} = \sqrt{2N}\gamma_w/M_s$$

Domain Wall Pinning at Inclusions and Voids

In developing new magnetic materials the control of the microstructure is of primary importance. Nonmagnetic grain boundaries are essential for magnetic recording media in decreasing the exchange coupling between grains; the properties of permanent magnets are defined through inclusions of phases with magnetic properties different from that of the matrix, while soft magnetic materials should be as homogenous as possible. In case of nonmagnetic inclusions or voids, the DW is pinned because the local DW energy is reduced by the missing volume when the DW includes the inclusion or void. At the same time, depending on the size of the defects, there will be free magnetic poles on the surface of the inclusions and voids, producing demagnetizing (stray) fields with a significant energy contribution (10,16,17,18,19).

Small Inclusions, $d \ll \delta_w$. When a spherical inclusion of size d, volume $v = \pi d^3/6$, is located outside of the DW it behaves like a dipole, having a dipole energy of $W_D \approx (1/3)\ M_s^2 v$. If it is inside of the DW, then it behaves as a quadrupole, and $W_Q = W_D/2$. If the interaction depends only on the distance between the inclusion (or void) and DW, then $d\gamma_w/dx \approx d^3\gamma_w/\delta_w^2$, and the critical field for the start of the DW motion, due to the volume effect for $d \ll \delta_w$ is given by (10):

$$H_{cr}^{i} = \frac{2.8\gamma_w}{M_s w}\left[\frac{d}{\delta_w}\right]^{3/2} v^{1/2}\left[\ln\frac{2w}{\delta_w}\right]^{1/2}$$

The contribution due to the demagnetizing field effects:

$$H_{cr}^{D} = \frac{2.8M_s d^{7/2}}{w\delta_w^{5/2}} v^{1/2}[\ln(2w/\delta_w)]^{1/2}$$

The critical fields H_{cr}^{i} and H_{cr}^{D} are comparable when $d \approx \delta_w/4$.

Large Inclusions, $d \gg \delta_w$

For large inclusions there would be a very large demagnetizing field contribution due to the strong dependence on the size of the inclusions, which is disadvantageous from the point of view of energy minimalization. The consequence is that a wedge-shaped secondary domain structure is developed around large inclusions to dilute the density of free poles over

a larger surface of the new DWs. The irreversible motion of the DW starts before it would be completely torn off the inclusion, at a field:

$$H_{cr}^{I} = \gamma_w v^{2/3}/(2M_s d)$$

The theory of inclusions was originally developed for spherical inclusions. The case of elliptical inclusions was treated in Refs. 18 and 19, showing that the strongest demagnetizing field effects are due to flat inclusions lying perpendicular to the plane of the DW. The critical field is for the case of extended planar inclusions, width d, including magnetic inclusions, H_{cr} depends on the relative magnitude of the anisotropy and exchange constants of the two materials (A and A', and K and K'), and it is given in Ref. 20:

$$H_{cr}^{i} = \frac{2Kd}{3^{3/2}M_s\delta_w}[A/A' - K'/K], \quad for\ d \ll \delta_w$$

$$H_{cr}^{i} = \frac{KA'}{2M_sA}[A/A' - K'/K], \quad for\ d \gg \delta_w$$

The calculation of critical fields can be solved analytically for simple cases only (21,22,23). Numerical methods of micromagnetism are very powerful in calculating the critical fields for DW pinning for any geometry and combination of defects. The most cumbersome part of the calculation, the magnetostatic fields due to the nonzero divergence of magnetization at the defects, can be handled easily by numerical methods. Details of the pinning process can be revealed by these methods, like the repulsion of the approaching DW by the dipole field of small inclusions in high magnetization materials (24,25). Figure 5 shows the domain structure of a garnet single crystal in $H \gg H_c$, near to saturation, where the strongest defects keep the last DWs pinned (26,27,28).

IRREVERSIBLE MAGNETIZATION PROCESSES

In a ferromagnet with a domain structure irreversible magnetization takes place by DW motion, due to the sudden changes of the magnetization as the applied magnetic field reaches the critical field of depinning a DW from a defect, as given in the previous section. On reducing the size of the magnetic body down to the typical size of a single domain, no DW can be formed and, consequently, there is no DW motion, and no irreversible losses associated with it. However, there are still irreversible magnetization changes due to the sudden rotation of the magnetic moment of the single-domain particles at the switching field of the particle. The sequence of individual rotation events of particle magnetizations gives rise to the hysteresis loops of particulate materials, usually described by Preisach models (1,7,29). The energy barrier for magnetization switching is related to the effective anisotropy field of the particles: $H_{cr}^{rot} = 2\,K_{eff}/M_s$, a fairly large value. These irreversible wall motion or rotational magnetization processes are the cause for the hysteresis losses. The measure of the energy loss associated with the hysteresis can be determined from the area under the hysteresis loop:

$$W_H = \oint_{\text{loop area}} H dM$$

The loss associated with an individual Barkhausen jump dW_B is determined in a similar way, by the area of the minor loop of one jump. Integrating over all individual jumps gives the total loss, W_H.

The shape of the hysteresis loop is expected to be determined by the sequential events of depinning the DWs from the defects, or the sequence of the individual switching events of particles by rotation. The sequence would depend only on the strength of the interaction between a defect and a DW. In this case the shape of the hysteresis loop would be reproducible and no random noise would be associated with the magnetization process. At the absolute zero of temperature $T = 0$ K, with no interaction between the particles, this could be a valid assumption. However, the shape of the hysteresis loop and the associated losses are influenced by several other irreversible processes. First of all, at *finite temperatures* temperature fluctuations add a random noise to the magnetization process, randomly raising or decreasing the energy barriers what the moving DW should overcome in order to change the magnetization (30,31). Moreover, the height of the barrier, that is, the strength of the interaction between the DW and the defect, might depend on the temperature itself.

At any given temperature if one waits long enough there will be a finite probability that a temperature fluctuation appears, large enough to push the DW over the next barriers. This characteristic time delay between an instantaneous change in the applied field and the subsequent change of the magnetization is the magnetic aftereffect (4,30). The higher the temperature the more effective is the assistance of temperature fluctuations. The slower the change of the field, the more chance the DW has to jump over the energy barrier, waiting for the moment of the temperature fluctuation assisted decrease in the energy barrier. The critical field of the start of the DW motion at one given defect depends on the temperature and time: $H_{cr} = H_{cr}(T, t)$. As a result, the faster the rate of change of the field, the larger the field needed to change the magnetization, that is, the coercivity H_c is increasing with frequency. The defect-DW interaction is influenced by the aftereffect, leading to an apparent frequency dependence.

Another effect that can't be neglected is the shape and size dependence of the magnetization curve. If a magnetic body of finite size is magnetized, free magnetic poles occur on the surface, producing demagnetizing field, H_d, which opposes the direction of the magnetization. The demagnetizing field is proportional to the magnetization, $\boldsymbol{H_d} = -N\boldsymbol{M}$, where N is the demagnetizing factor (1,2,32). When the magnetization changes in a small region of the body, the demagnetizing field changes too, and the slope of the hysteresis loops changes, depending on the demagnetizing factor and the permeability $\mu = \boldsymbol{dB}/\boldsymbol{dH} = \boldsymbol{d}(\mu_0\,\boldsymbol{H} + \boldsymbol{M})/\boldsymbol{dH}$. This change causes an apparent change in the magnetization at a given applied field. A more serious problem is that the magnetic body is not homogeneously magnetized. The direction and the magnitude of the domain magnetizations vary, and the permeability is not a well-defined quantity. The effect of the sample's shape and size makes the comparison of experimental data very difficult.

Eddy current losses can't be neglected in the case of ac magnetization processes of metallic magnets. When the magnetization is changed in a conductor, eddy currents and, associated with it, a time-dependent magnetic induction $B(t)$ is produced. Integrating $B(t)$ over the sample surface, the

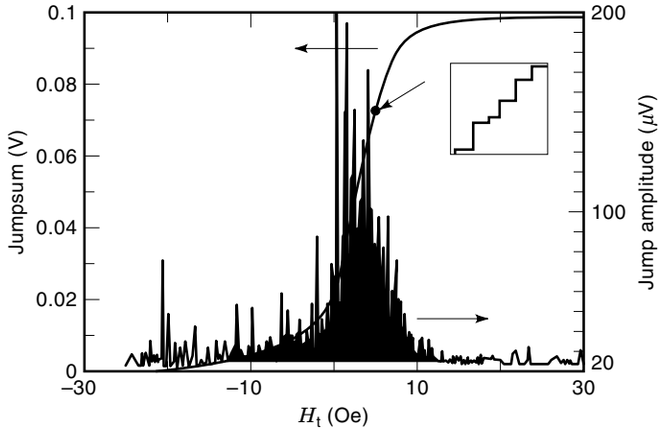

Figure 10. Barkhausen jump statistics of a low carbon steel specimen, and the integrated jumpsum signal. The inset is the measured signal at higher magnification. (Courtesy of L. J. Swartzendruber, NIST, unpublished data).

change of the flux in time, that is, the voltage induced by the eddy current is obtained. Due to interference from this eddy-current induced signal, the measurement of the Barkhausen noise in metallic magnets is not a simple task (33).

BARKHAUSEN NOISE

Any discontinuous, sudden change of the magnetization in a slowly changing magnetic field, due to the irreversible breakaway of a DW from a pinning center or an irreversible act of rotation, induces a voltage spike in a coil surrounding the specimen. The sequence of these pulses is the Barkhausen noise. The pulses are characterized by their number in the applied field interval, magnitude of the induced voltage, width of the pulse, and the integrated voltage, the *jumpsum.* The change of the magnetization during one jump is related to the integral under the area of the resultant pulse. The steepest part of the hysteresis loop, around the coercivity H_c contains the largest number and highest amplitude pulses. The defect structure influences both mechanical and magnetic properties of the materials. The distribution of jump size, shape, duration, and the power spectrum of the Barkhausen noise is directly related to the microstructure of the magnetic material, and carries very important information for nondestructive testing. Figure 10 shows the applied magnetic field dependence of the Barkhausen noise data for a steel specimen in terms of pulse heights of the induced voltage, and the integrated voltage (jumpsum), which is related to the magnetization (33).

Stress Effects

The defect DW interaction is very sensitive to the stress due to stress-induced anisotropy in materials with finite magnetostriction. Upon an application of stress the DW energy landscape and the critical field for individual DW jumps change and, as a result, the shape of the hysteresis loop and the permeability change with stress as well. After proper calibration, and over a wide range of stress, the Barkhausen noise can often be used as a measure of the strain state of the material (34,35).

In materials with strong uniaxial anisotropy, the equilibrium domain structure is relatively simple. In a stressed long wire or ribbon, domain magnetizations will be aligned along the long axis and the magnetization process is dominated by one huge Barkhausen jump. The hysteresis loop of such a material is nearly square. For a wire with large magnetostriction, $\lambda > 0$, under tensile stress σ along the axis, there is a stress-induced uniaxial anisotropy: $K_s = (3/2)\sigma\lambda$. The large change in magnetic induction upon changing the magnetic field will induce a large, narrow pulse of voltage in a coil wound around the sample, used in many sensors and devices. Stress can be induced in amorphous magnetostrictive wires during heat treatment, and can be used as inductors. Figures 11 and 12 show the effect of magnetostriction and mechanical stress on Barkhausen noise statistics upon magnetization of a highly magnetostrictive amorphous metallic ribbon in a free state and when the same ribbon is slightly stretched along its axis (36). The change of the Barkhausen jump spectrum from

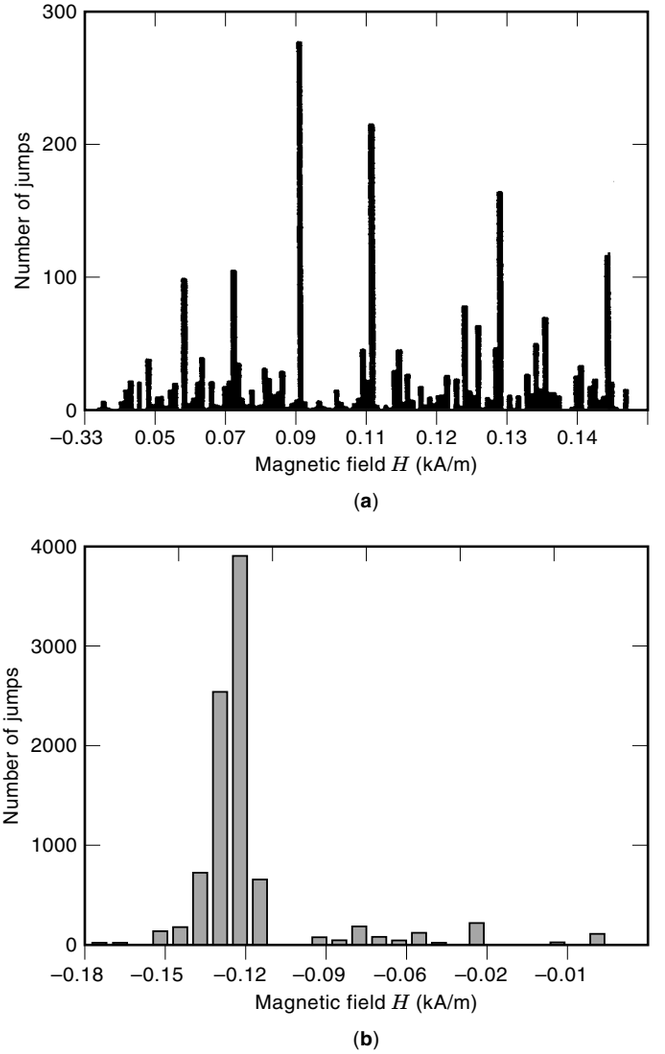

Figure 11. Effect of magnetostriction and mechanical stress on Barkhausen noise statistics upon magnetization of a highly magnetostrictive amorphous metallic ribbon (a) Free ribbon; (b) Ribbon under weak tensile stress (M. Pardavi-Horvath, unpublished data).

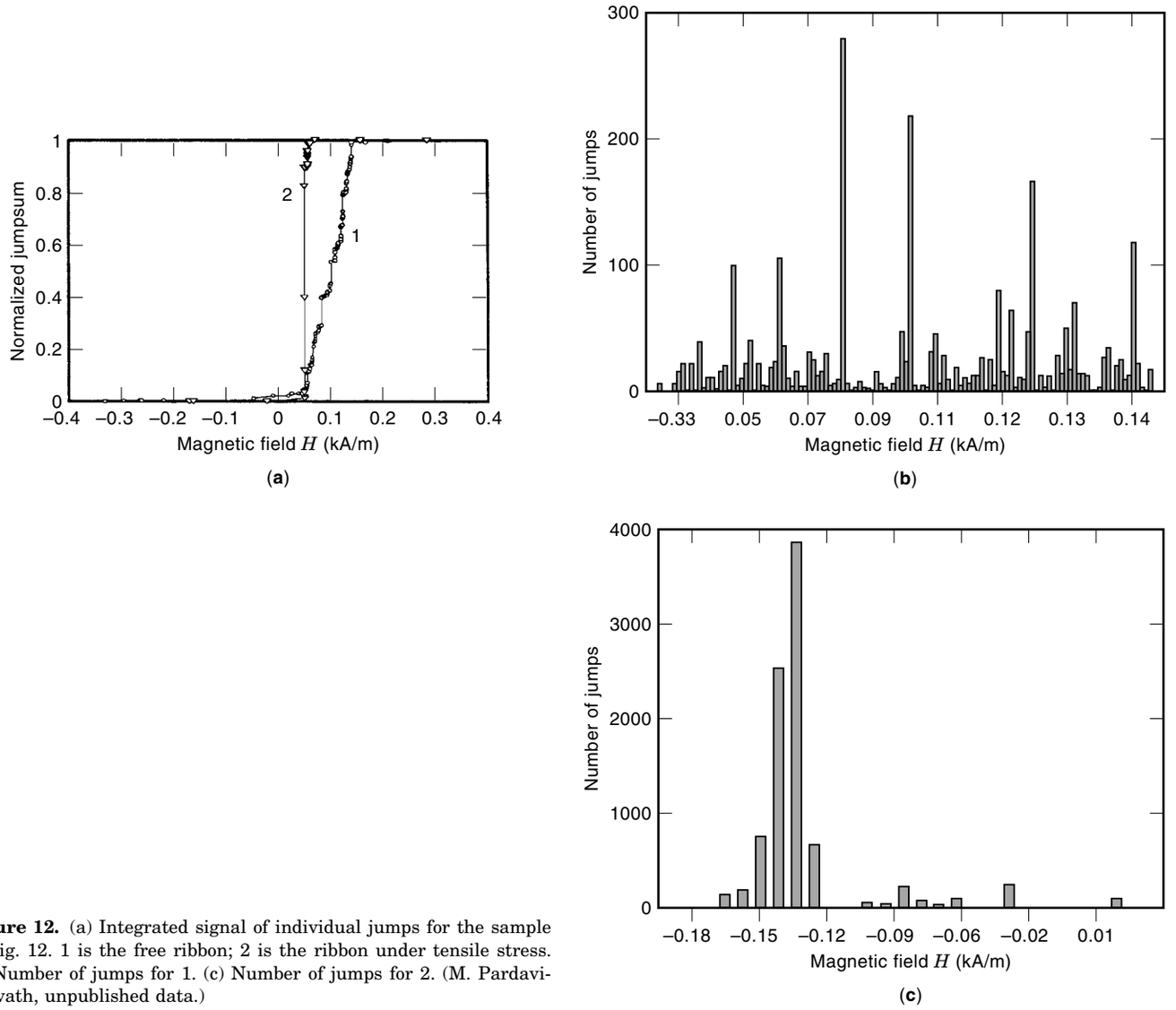

Figure 12. (a) Integrated signal of individual jumps for the sample in Fig. 12. 1 is the free ribbon; 2 is the ribbon under tensile stress. (b) Number of jumps for 1. (c) Number of jumps for 2. (M. Pardavi-Horvath, unpublished data.)

numerous small jumps to a very few huge jumps is evident. The integral of the jumps over the magnetic field gives a curve similar to the magnetization curve (37).

Temperature Dependence

The Barkhausen effect has a strong temperature dependence. The DW energy itself depends on the magnetic anisotropy, a strong function of temperature, leading to the increase of the DW energy and the coercivity on lowering the temperature. The energy of temperature fluctuations play a lesser role at low temperatures, and the characteristic time constant of the magnetic aftereffect is increasing with decreasing temperature. As the probability for a jump decreases, the DW has to wait longer for a kick from the thermal fluctuations, and the number of jumps in a given field and time interval decreases (33). On the contrary, upon increasing the temperature the coercivity decreases, and due to strong thermal activation processes, it's easier for a DW to make a jump. At the same time the thermal energy becomes larger than some of the DW-defect interaction energies, many of the low energy defects are "turned off"' and the width of the defect-DW interaction spectrum decreases too. The magnetic material becomes magnetically softer.

Statistics of Barkhausen Jumps

The statistics of Barkhausen jumps has been the topic of wide ranging investigations for many years. The static interaction of *one* defect with *one* domain wall is just the beginning of the theoretical treatment of the magnetization process of a magnetic material. In a real material, a very large number of statistically distributed defects interact with a large number of DWs, resulting in a complex Barkhausen noise behavior. The process depends on temperature, time, sample size, and shape (38,39). For the interpretation of the Barkhausen signal the functional form of the energy landscape is needed. All these unknown parameters can be taken into account as fluctuations in the DW energy, and described by an ensemble of stochastic Langevin functions. The model generates both

hysteresis loops and Barkhausen jump distributions, showing a power-law behavior for small jumps and a rapid cut-off at large jump sizes, in agreement with the experimental data (40,37,41).

Unfortunately, along the hysteresis loop different types of magnetization processes take place. Therefore, the treatment is usually restricted to the constant permeability region around the coercivity. The assumption used in predicting the noise power spectrum (42) is that both dB/dH and dH/dt are constant. This approach was extended to the whole hysteresis loop assuming that the Barkhausen activity in terms of the jumpsum is proportional to the differential susceptibility, which can be determined from hysteresis models (43).

An important question is whether the individual jumps are correlated or not. For statistically independent jumps the theory predicts that the power density is constant at low frequencies and decays as $1/f^2$ at high frequencies. Some experimental data agree with this prediction, however, in some cases there is a maximum at low frequencies. The analysis of the Barkhausen noise signal characteristics, as autocorrelation, jump amplitude correlation, jump time and amplitude correlation, and power density show no evident deviation from random noise behavior. Evidently, a different mechanism is responsible for the low frequency losses (44).

The progress in nonlinear dynamics and chaos, relatively easily applicable to the behavior of domains and domain walls, leads to simple nonlinear models for DW dynamics, taking into account the viscous damping of the DW moving under the effect of a harmonic external force in the field of defects. It was shown that Barkhausen noise can be characterized by a low fractal dimension (45,46). Barkhausen jumps show the attributes of self-organized criticality, with the distribution of lifetimes and areas of discrete Barkhausen jumps following a power-law behavior (47,48).

Experimental Techniques

Modern Barkhausen spectrometers are based on the same principle of Faraday's law of induced electromotive force (emf), as used by Barkhausen in 1919. According to Faraday's law, whenever there is a magnetic flux change dB/dt there will be an induced voltage V, proportional to dB/dt and the number of turns of a measuring pickup coil. The difference is that the original amplifier is now substituted by a digital computer controlled data acquisition system and digital storage oscilloscope (33,44,49). Usually the size and the duration of Barkhausen pulses is measured and statistically registered. The results are frequency distributions. The entire sequence of Barkhausen pulses can be considered as a stochastic process and then the spectral density of the noise energy, related to the total irreversible magnetization reversal is measured (33,39). Figure 13 shows the block diagram of a typical apparatus. The equipment consists of a magnetizing system used to sweep the sample through the full hysteresis loop from negative saturation to positive saturation, at a frequency of typically 0.05 Hz; a Hall probe to measure the magnetic field; a surface coil to measure the induced voltage and/or another pick-up coil, surrounding the sample, for power spectrum measurements. The measurement is controlled and the data are analyzed by a digital computer. The bandwidth of the system is from 100 Hz up to 100 kHz. A discriminator is used to reject signals below a certain noise level. At each instant of time, t_n, the value of the magnetic field, H_n and the induced voltage is V_n measured. So the amplitude of jumps versus field, the integrated signal, the jumpsum, and the rate of the jumpsum can be determined. The jumpsum rate is qualitatively similar to the rms noise. Power density spectra and autocorrelation functions can also be obtained from the data. For a stationary random process, the power density spectrum is the Fourier transform of the autocorrelation function, $\Phi(t) = \langle V(t) \times V(t + \tau) \rangle$, so that statistical properties of the Barkhausen noise can be easily investigated by this technique (49).

A widely used method in studying the Barkhausen effect is to measure the power as a function of the frequency of cycling the field. This technique yields information about the intervals between jumps (33). The frequency of the Barkhausen jumps is related to the average DW velocity, and it contains information about the average time it takes for a moving DW to reach the next barrier through the average distance between defects.

Utilizing the optical activity of magnetic materials it is possible to identify individual defects, pinning mechanisms, and measure actual DW velocities. In transparent magnetic materials individual DW-defect interactions can be investigated via the magneto-optical Faraday-effect (26,27,28), as illustrated in Figs. 2, 6, 7, and 9. In metals, the Kerr effect offers a possibility to visualize the defect-DW interaction, as it was done for several metallic film magneto-optical recording media, in order to study the cause of media noise in readout (50). It was shown that the distance between pinning centers is about 0.4 μm and the DW "waits" up to several seconds before the next jump. The pinning time decreases exponentially with increasing driving field.

Nondestructive Testing

When applicable the measurement of magnetic Barkhausen noise is a fast, reliable, and simple technique for nondestruc-

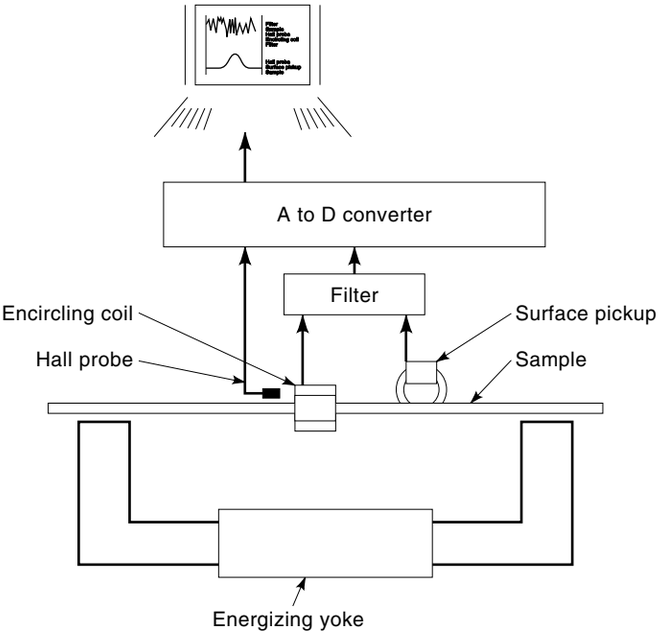

Figure 13. Block diagram of Barkhausen noise measurement. (Courtesy of L. J. Swartzendruber, NIST.)

tive material evaluation, as compared to x-ray diffraction, ultrasound, and other more sophisticated measurements (49,51). The Barkhausen effect is especially well-suited for the study of steel, one of the most important structural materials. Commercial instruments to characterize materials based on Barkhausen noise are now available. The Barkhausen spectrum can be, for example, related to the grain size of the material, so it can be used for grain size measurement after cold-rolling (52). The stress sensitivity of the DW motion makes it very convenient to study residual stresses, using the Barkhausen emission under stress. Depending on the bandwidth of the measurement, either the surface or near subsurface layers can be tested (34). The Barkhausen emission test is used in the grinding industry to check the residual stress due to thermal damage and microhardness (53). Plastic deformation increases the dislocation density, an effect easily detected by the DW-dislocation interaction induced critical field increase. There is a possibility to use deformed thin wires of iron and iron–nickel alloys as strain gages in the 10^{-3} range with a sensitivity of $\pm 5\%$ (35).

Barkhausen noise plays an important role in magnetic recording. The head-to-medium velocities in hard drives may range from 1 to 50 m/s, with data frequencies from 100 kHz to 50 MHz; for tape systems the velocity might be as low as 25 mm/s at 1 Hz frequency. These parameters are very near to the range of Barkhausen noise. The main source of the medium and head noise is the Barkhausen noise. The nonuniformity of media leads to a localized, regular noise, superimposed on the random noise from magnetization switching processes. For particulate materials the noise is related to the shape, size, and orientation dispersion of the particles; for multigrain thin film media the signal-to-noise ratio (SNR) depends on the microstructure, texture, and grain cluster size. In soft magnetic write-read head materials the DW pinning and the related hysteresis losses are the most important source of noise (50,54).

FLUX PINNING AND LOSSES IN SUPERCONDUCTORS

The basic parameters defining the transition from the superconducting to the normal state are the critical temperature T_c, critical magnetic field H_c, and critical current density J_c. Type II superconductors possess the highest possible critical parameters. Destruction of their bulk superconductivity occurs at the upper critical field H_{c2}. If no applied magnetic field is present, then J_c up to 10^{11} Am^{-2} can be reached. High current density and small energy dissipation is the main reason for industrial applications of superconductors in magnets, electrical machinery, and power transmission lines. Ideal superconductors are lossless, however, using Type II superconductors for practical applications dissipative processes are of great importance. In Type I superconductors dissipation is negligible up to very high frequencies, where the electromagnetic field destroys the Cooper pairs, responsible for superconductivity. Losses in ideal Type II superconductors are associated with viscous motion of vortex lattices. Losses in the most important class of superconductors, the Type II nonideal superconductors, are due to magnetic hysteresis, similar to the case of ferromagnetic materials. In superconductors the irreversible motion of magnetic flux lines through pinning centers causes the hysteresis. The problem is more complicated in technical materials: superconducting cables are multifilament, multicore, twisted, stabilized composites where the coupling losses to the normal matrix play a significant role in dissipation (55).

Vortex Structure

Superconductors (SC) are characterized by the penetration depth of the weak magnetic field λ, the coherence length ξ, and the Ginzburg-Landau parameter $\kappa = \lambda/\xi$. Superconductors can be classified according to the magnitude of κ. Type I SCs have $\kappa < 1/\sqrt{2}$, and the external field is totally screened by diamagnetic supercurrents flowing in the penetration depth distance from the surface (Meissner effect). For Type II SCs $\kappa > 1/\sqrt{2}$. The N/S boundary is in equilibrium only in high applied magnetic field. A type II SC below the first critical field H_{c1} behaves as a Type I material. In a field of $H > H_{c1}$ it is energetically more favorable to break into the mixed state of alternating N and SC phases, consisting of thin, normal core vortex lines, parallel to the external field, with circulating paramagnetic supercurrents. Each vortex carries a quantum of flux $\phi_0 = hc/2e$, where h is the Planck constant, c is the light velocity and e is the electron charge. The size of a vortex is typically a few hundred nanometer. The vortex lattice is in some way analogous to the magnetic domain structure of ferromagnetic materials, as discussed previously. Upon increasing the applied magnetic field H, the number of vortices increases as the vortex lattice period becomes smaller. At $H = H_{c2} = \sqrt{2}\ \kappa H_c$ the vortex cores overlap and the material becomes a normal metal. H_{c2} of SC for practical applications is on the order of 10^2 T.

Vortex Motion and Flux Jumps

Many technical applications of SC require high current densities and low losses, which can be accomplished by immobilizing the vortices by pinning them at defects. The vortices have a complex magnetic field around them, decaying exponentially within the distance λ. If the SC is placed in an applied field H, parallel to its surface, then supercurrents J_m will be generated by a vortex located at x_0:

$$J_m = \lambda^{-1} H \exp(-x_0/\lambda)$$

and a repulsive Lorentz force will act on the vortex, $F_m = J_m \phi_0$. This force changes with the distance, thus changing the free energy of the vortex system. If there is an energy gradient, that is, a local change in the potential for the vortex motion, then the vortex can be pinned at the defect lowering the free energy of the system. There is an energy barrier to the penetration of vortices in and out of the SC at the boundary, and vortex motion into the SC can be prevented by surface treatment. Ideal Type II SCs are thermodynamically reversible if there are no defects in the material to act as pinning centers. But even in the absence of bulk pinning, there is always the surface, itself an irregularity, so there is no ideal SC. In the absence of pinning centers, the vortex lattice's motion is like a hydrodynamic flow in a viscous medium. Dissipation is due to the viscous damping process. The power necessary to move the vortices is $W_{SC} = \rho_n J_s^2$, where ρ_n is the specific resistance. Because there are always thermal fluctuations, and J_c is decreasing with increasing T, any slight increase in the temperature decreases the critical current and,

by preserving the total current, the current distribution has to change, and as a consequence, the magnetic field distribution generated by the current distribution is changes too. According to Maxwell's law whenever there is a flux change there will be an electric field, and this field does the work to move the vortices, that is, a flux jump is observed. Flux jump instabilities are very dangerous because they can transform the SC into the N state completely. Thermally activated flux flow is one of the main reasons for the low current density in new high-T_c SCs.

Another case of flux jumping occurs due to magnetic field fluctuations. As the applied field increases, critical shielding currents are induced to prevent the penetration of flux into the SC until a certain field H^* (or magnetic flux density associated with that field B^*) value , where flux jumps occur. For thin filaments the flux completely penetrates the material, and there is no flux jumps even for applied fields much greater than H^*. The constraint on the thickness d of the SC material is that:

$$\mu_0 J_c d < B^* = [3\mu_0 S(T_c - T)]^{1/2}$$

where S is the volume heat capacity of the material (56).The distribution of the induction is usually described by the Bean-London model of critical state, where the magnitude of the critical current is directly related to the gradient of the local induction $J_c = dB/dx$. A change in the penetration occurs only when the change in the external field exceeds the surface shielding fields created by shielding currents, according to Maxwell's equations. This picture of SC hysteresis losses is valid up to about 10^3 Hz. In the Bean–London model the contribution of the vortex structure is not included. A complete analytical solution for the distribution of current and induction in hard SCs is still missing.

Nonideal Type II SCs

Real materials always have spatial inhomogeneities acting as pinning centers that prevent the penetration of flux into the SC upon increasing the applied field; or preventing the exclusion of flux upon decreasing field, giving rise to hysteresis and associated irreversible losses. There is a remanence flux frozen in the SC even in the absence of external field. In analogy with hard magnets, these nonideal Type II SCs are called *hard SCs.*

The pinning centers are similar to those in magnetic materials, preventing the motion of domain walls, such as: point defects of inclusions, voids, precipitates of second phase, line defects like dislocations, grain boundaries, twin boundaries, and so on. The bigger the difference between the properties of the defect and the SC the larger is the pinning effect, again similar to the case of the strong DW pinning for high DW energy gradient in ferromagnets.

There is no complete, exact theory of pinning in SCs, and the methods used to describe the vortex-defect interactions are very similar to those dealing with DW pinning. Strong pinning and high current density is achieved mostly by microstructural developments through technology of preparation, compositional modifications, and different treatments (for example, irradiation). In intermetallic SCs (Nb_3Sn, Nb_3Ge) the pinning centers are related to the fine grained structure on the order of a few nm, and precipitation of oxides or carbides at grain boundaries. In the high-T_c cuprate SCs vortex pinning is linked to the layered structure of the material, the vortices are interacting strongly within the layers (pancake vortices) and weakly between layers. As a result the electrical properties are highly anisotropic. The pancake vortices are very mobile. Increasing the interlayer coupling would make a more effective pinning with higher (and isotropic) current densities (57).

In an ideal SC the vortex structure is a regular two-dimenisonal network. Due to the very inhomogeneous structure of the hard SCs, the vortex lattice is distorted, following the microstructural features, that is, the energy landscape of the material. For high defect densities and high current densities the vortex lattice becomes "amorphous", the lattice is "melted".

BIBLIOGRAPHY

1. Soshin Chikazumi and Stanley H. Charap, *Physics of Magnetism,* New York: Wiley, 1964.
2. Richard M. Bozorth, *Ferromagnetism,* New York: IEEE Press, 1993.
3. Ami E. Berkowitz and Eckart Kneller (ed.), *Magnetism and Metallurgy,* New York: Academic Press, 1969.
4. H. Kronmüller, *Magnetisierunskurve der Ferromagnetika* I. In Alfred Seeger (ed.), *Moderne Probleme der Metallphysik,* Vol. 2, Ch. 8, Berlin: Springer Verlag, 1966.
5. H. Träuble, *Magnetisierungskurve der Ferromagnetika* II. In Alfred Seeger (ed.), *Moderne Probleme der Metallphysik,* Vol. 2, Ch. 9, Berlin: Springer Verlag, 1966.
6. M. Pardavi-Horvath and Hyunkyu Kim, Surface roughness effects on the coercivity of thin film heads. *J. Korean Magn. Soc.,* **5**: 663–666, 1995.
7. M. Pardavi-Horvath, A simple experimental Preisach model system. In G. Hadjipanayis (ed.) *Magnetic Hysteresis in Novel Magnetic Materials,* Amsterdam: Kluwer Publ., 1997.
8. J. A. Jatau, M. Pardavi-Horvath, and E. Della-Torre, Enhanced coercivity due to local anisotropy increase. *J. Appl. Phys.,* **75**: 6106–08, 1994.
9. H. Träuble, in Ref. 3, pp. 622–685.
10. H. Träuble, in Ref. 5, pp. 257–279.
11. Martin Kersten, Über die Bedeutung der Versetzungsdichte für die Theorie der Koerzivkraft rekristallisierter Werkstoffe, *Z. Angew Phys.,* **8**: 496–502, 1956.
12. K.-H. Pfeffer, Zur Theorie der Koerzitivfeldstärke und Anfangssusceptibilität, *Phys. Stat. Sol.,* **21**: 857–872, 1967.
13. K.-H. Pfeffer, Wechselwirkung zwischen Versetzungen und ebenen Blochwänden mit starrem Magnetisierungsverlauf, *Phys. Stat. Sol.,* **19**: 735–750, 1967.
14. K.-H. Pfeffer, Mikromagnetische Behandlung der Wechselwirkung zwischen versetzungen und ebenen Blochwänden, *Phys. Stat. Sol.,* **21**: 837–856, 1967.
15. Horst-Dietrich Dietze, Theorie der Blochwandwölbung mit Streufeldeinfluss. *Z. Phys.,* **149**: 276–298, 1957.
16. L. J. Dijkstra and C. Wert, Effect of inclusions on coercive force of iron, *Phys. Rev.,* **79**: 979–985, 1950.
17. R. S. Tebble, The Barkhausen effect. *Proc. Phys. Soc., London,* **B86**: 1017–1032, 1995.
18. E. Schwabe, Theoretische Betrachtungen über die Beeinflussung der ferromagnetischen Koerzivkraft durch Einschlüsse mit rotationellelliptischer Form, für den Fall, dass deren Abmessungen klein gegen die Dicke Blochwand sind, *Ann. Physik,* **11**: 99–112, 1952.

19. K. Schröder, Magnetisierung in der Umgebung unmagnetischer Einschlüsse in Ferromagnetika, *Phys. Stat. Sol.,* **33**: 819–830, 1969.
20. D. I. Paul, Extended theory of the coercive force due to domain wall pinning, *J. Appl. Phys.,* **53**: 2362–2364, 1982.
21. P. Gaunt, Ferromagnetic domain wall pinning by a random array of inhomogeneities, *Phil. Mag. B,* **48**: 261–276, 1983.
22. Xinhe Chien and P. Gaunt, The pinning force between a Bloch wall and a planar pinning site in MnAlC, *J. Appl. Phys.,* **67**: 2540–2542, 1990.
23. Wolfgang Prause, Energy and coercive field of a porous ferromagnetic sample with Bloch walls. *J. Magn. Magn. Mater.,* **10**: 94–96, 1979.
24. M. A. Golbazi et al., A study of coercivity in Ca-Ge substituted epitaxial garnets, *IEEE Trans. Magn.,* **MAG-23**: 1945, 1987.
25. E. Della Torre, C. M. Perlov, and M. Pardavi-Horvath, Comparison of coercivity calculations of anisotropy and exchange wells in magnetooptic media, *J. Magn. Magn. Mater.,* **104–107**: 303–304, 1992.
26. M. Pardavi-Horvath, Defects and their avoidance in LPE of garnets, *Progress in Crystal Growth and Characterization,* **5**: 175–220, 1982.
27. M. Pardavi-Horvath, Coercivity of epitaxial magnetic garnet crystals, *IEEE Trans. Magn.,* **MAG-21**: 1694, 1985.
28. M. Pardavi-Horvath and P. E. Wigen, Defect and impurity related effects in substituted epitaxial YIG crystals, Advances in Magneto-Optics, *J. Magn. Soc. Jpn.,* **11**: S1, 161, 1987.
29. Franz Preisach, Untersuchungen über den Barkhauseneffekt, *Ann. Physik,* **5**: 737–799, 1929.
30. Isaak D. Mayergoyz and Can E. Korman, Preisach model with stochastic input as a model for magnetic viscosity, *J. Appl. Phys.,* **69**: 2128–2134, 1991.
31. I. D. Mayergoyz and G. Friedman, The Preisach model and hysteretic energy losses, *J. Appl. Phys.,* **61**: 3910–3912, 1987.
32. Xiaohua Huang and M. Pardavi-Horvath, Local demagnetizing tensor calculation for rectangular and cylindrical shapes, *IEEE Trans. Magn.,* **32**: 4180–4182, 1996.
33. John C. McClure, Jr. and Klaus Schröder, The magnetic Barkhausen effect, *CRC Critical Rev. Solid State Sci.,* **6**: 45–83, 1976.
34. D. C. Jiles, P. Garikepati, and D. D. Palmer, Evaluation of residual stress in 300M steels using magnetization, Barkhausen effect and X-ray diffraction techniques. In Donald O. Thompson and Dale E. Chimenti (Eds.) *Rev. Progr. Quantitative Nondestructive Evaluation,* **8B**: 2081–2087, Plenum Press: New York, 1989.
35. A. H. Wafik, Effect of deformation on Barkhausen jumps of fine wires of iron, nickel and iron-nickel alloy, *J. Magn. Magn. Mater.,* **42**: 23–28, 1984.
36. M. Pardavi-Horvath, unpublished data.
37. R. D. McMichael, L. J. Swartzendruber, and L. H. Bennett, Langevin approach to hysteresis and Barkhausen jump modeling in steel, *J. Appl. Phys.,* **73**: 5848–5850, 1993.
38. Richard M. Bozorth, Barkhausen effect in iron, nickel and permalloy. I. Measurement of discontinuous change in magnetization, *Phys. Rev.,* **34**: 772–784, 1929.
39. U. Lieneweg and W. Grosse-Nobis, Distribution of size and duration of Barkhausen pulses and energy spectrum of Barkhausen noise investigated on 81% nickel-iron after heat treatment, *Int. J. Magn.,* **3**: 11–16, 1972.
40. B. Alessandro et al., Domain-wall dynamics and Barkhausen effect in metallic ferromagnetic materials, *I. Theory, J. Appl. Phys.,* **68**: 2901–2907, 1990.
41. F. Y. Hunt and R. D. McMichael, Analytical expression for Barkhausen jump size distributions, *IEEE Trans. Magn.,* **30**: 4356–4358, 1994.
42. G. Bertotti, G. Durin, and A. Magni, Scaling aspects of domain wall dynamics and Barkhausen effect in ferromagnetic materials, *J. Appl. Phys.,* **75**: 5490–5492, 1994.
43. D. C. Jiles, L. B. Sipahi, and G. Williams, Modeling of micromagnetic Barkhausen activity using a stochastic process extension to the theory of hysteresis, *J. Appl. Phys.,* **73**: 5830–5832, 1993.
44. L. J. Swartzendruber et al., Barkhausen jump correlations in thin foils of Fe and Ni, *J. Appl. Phys.,* **67**: 5469–5471, 1990.
45. B. Alessandro, G. Bertotti, and A. Montorsi, Phenomenology of Barkhausen effect in soft ferromagnetic materials, *J. Physique,* **49** (C8): 1907–1908.
46. H. Yamazaki, Y. Iwamoto, and H. Maruyama, Fractal dimension analysis of the Barkhausen noise in Fe-Si and permalloy, *J. Physique,* **49** (C8): 1929–1930.
47. P. J. Cote and L. V. Meisel, Self-organized criticality and the Barkhausen effect. *Phys. Rev. Lett.,* **67**: 1334–1337, 1991.
48. J. S. Urbach, R. C. Madison, and J. T. Markert, Reproducibility of magnetic avalanches in an Fe-Ni-Co magnet, *Phys. Rev. Lett.,* **75**: 4964–4967, 1995.
49. L. J. Swartzendruber and G. E. Hicho, Effect of sensor configuration on magnetic Barkhausen observations, *Res. Nondestr. Eval.,* **5**: 41–50, 1993.
50. S. Gadetsky and M. Mansuripur, Barkhausen jumps during domain wall motion in thin magneto-optical films, *J. Appl. Phys.,* **79**: 5667–5669, 1996.
51. G. V. Lomaev, V. S. Malyshey, and A. P. Degterev, Review of the application of the Barkhausen effect in nondestructive inspection, *Sov. J. Nondestructive Testing,* **20**: 189–203, 1984.
52. S. Titto, M. Otala, and S. Säynäjäkangas, Non-destructive magnetic measurement of steel grain size. *Non-Destructive Testing,* **9**: 117–120, 1976.
53. H. Gupta, M. Zhang, and A. P. Parakka, Barkhausen effect in ground steel, *Acta Mater.,* **45**: 1917–1921, 1997.
54. C. Denis Mee and Eric D. Daniel (eds.), *Magnetic Recording,* New York: McGraw-Hill, 1987.
55. V. Kovachev, *Energy Dissipation in Superconducting Materials,* Clarendon Press: Oxford, 1991.
56. Lawrence Dresner, *Stability of Superconductors,* Plenum Press: New York, 1995.
57. George W. Crabtree and David R. Nelson, Vortex physics in high-temperature superconductors, *Physics Today,* **38–45**: April 1997.

Reading List

A rich source of up-to-date information on Barkhausen noise, magnetic domain wall pinning, and hysteresis losses are the issues of the *J. Appl. Phys.,* and *IEEE Trans. Magn.,* publishing the material of the annual conferences on magnetism. The *IEEE Trans. Appl. Supercond.* is suggested as a source of current information on flux pinning in superconductors.

MARTHA PARDAVI-HORVATH
The George Washington University

MAGNETIC NONDESTRUCTIVE TESTING.

See MAGNETIC METHODS OF NONDESTRUCTIVE EVALUATION.